Mon. Not. R. Astron. Soc. **371,** 1681–1692 (2006) doi:10.1111/j.1365-2966.2006.10792.x

Short time-scale variability in the Faint Sky Variability Survey

L. Morales-Rueda,[1⋆] P. J. Groot,[1⋆] T. Augusteijn,[2⋆] G. Nelemans,[1⋆]
P. M. Vreeswijk[3,4⋆] and E. J. M. van den Besselaar[1⋆]

[1]*IMAPP, Department of Astrophysics, Radboud University Nijmegen, PO Box 9010, 6500 GL Nijmegen, the Netherlands*
[2]*Nordic Optical Telescope, Apartado 474, E-38700 Santa Cruz de La Palma, Spain*
[3]*European Southern Observatory, Alonso de Córdova 3107, Vitacura, Casilla 19001, Santiago 19, Chile*
[4]*Departamento de Astronomía, Universidad de Chile, Casilla 36-D, Santiago, Chile*

Accepted 2006 July 4. Received 2006 June 28; in original form 2006 May 17

ABSTRACT

We present the *V*-band variability analysis of the point sources in the Faint Sky Variability Survey on time-scales from 24 min to tens of days. We find that about one per cent of the point sources down to $V = 24$ are variables. We discuss the variability-detection probabilities for each field depending on field sampling, amplitude and time-scale of the variability. The combination of colour and variability information allows us to explore the fraction of variable sources for different spectral types. We find that about 50 per cent of the variables show variability time-scales shorter than 6 h. The total number of variables is dominated by main-sequence sources. The distribution of variables with spectral type is fairly constant along the main sequence, with 1 per cent of the sources being variable, except at the blue end of the main sequence, between spectral types F0 and F5, where the fraction of variable sources increases to about 2 per cent. For bluer sources, above the main sequence, this percentage increases to about 3.5. We find that the combination of the sampling and the number of observations allows us to determine the variability time-scales and amplitudes for a maximum of 40 per cent of the variables found. About a third of the total number of short time-scale variables found in the survey were not detected in either *B* or/and *I* band. These show a similar variability time-scale distribution to that found for the variables detected in all three bands.

Key words: methods: data analysis – surveys – stars: general – stars: statistics – stars: variables: other.

1 INTRODUCTION

There is a wide range of photometrically variable systems in the Universe. The range of time-scales on which these systems vary is as wide as the physical processes that produce their variability. For example, we have intrinsically variable stars, where the variability is caused by changes in their internal structure or atmosphere that vary with time-scales of minutes to years (Brown & Gilliland 1994). Other stars show variability because they rotate and their surface is inhomogeneous, for example, because of star spots (Brinkworth et al. 2005), or because they form part of a binary or multiple system and their revolution around the centre of mass of the system results in changes on the detected flux due to the changing aspect of a non-isotropically emitting surface or eclipses. This is also the case for planets orbiting stars. The time-scale of the variability in this case is dictated by the orbital parameters of the system and can range from seconds to years. Near-earth objects (NEOs), such as asteroids, also show variability as they rotate and are non-spherical. We find photometric variability in extragalactic objects as well, such as quasars, where the variability is probably the result of material being accreted by the central engine, or 'one of' systems, such as gamma-ray bursts (GRBs) or supernovae (SNe) where the variability is produced by intrinsic changes in the structure of an astronomical object that take place only once.

The study of variability provides important information about the physical nature of the variable objects, leads to the discovery of new classes of objects, helps to study the physical structure of stars, for example, pulsating stars, allows us to obtain information on Galactic structure through the use of variables such as RR Lyrae as standard candles, and is the key to determining extragalactic distances through the use of standard candles, such as Cepheids and Type Ia SNe.

Most of our knowledge of variability is based on the study of apparently bright sources, which naturally selects members of *intrinsically* bright populations. At present, little is known about variability of intrinsically fainter populations, because in bright samples they are lacking altogether or are only represented by a few members.

⋆E-mail: lmr@astro.ru.nl (LM-R); pgroot@astro.ru.nl (PJG); tau@not.iac.es (TA); nelemans@astro.ru.nl (GN); pvreeswi@eso.org (PMV); besselaar@astro.ru.nl (EJMvdB)

The Faint Sky Variability Survey (FSVS; Groot et al. 2003) was designed to account for this deficit by studying two unexplored regions of the variability space: the short time-scale variability region (down to tens of minutes) and the intrinsically faint variable sources (down to $V = 24$ mag) at mid and high Galactic latitudes. The FSVS also contains colour information for all targets, giving us the option of positioning objects in the colour–colour diagram, as well as finding the variability time-scales and amplitudes that characterize them. The main aims of the FSVS are thus to obtain a map of a region of the Galaxy ($\sim$21 deg^2) in variability and colour space, to determine the population density of the different variable objects that reside in the Galaxy and to find the photometric signature of up-to-now unknown intrinsically faint variable populations. In this paper, we explore these three goals.

There are other surveys that study the variable optical sky, each emphasizing one aspect or one particular region of this parameter space. The time-scales sampled, depth and sky coverage of different variability surveys vary depending on the astronomical objects they are designed to study. For example, with a brightness limit similar to the FSVS, Street et al. (2005) studied the variability around an open cluster with time-scales longer than a few hours, and Ramsay & Hakala (2005) studied the rapid variability (down to 2 min) of objects as faint as $V \sim 22.5$. Of great interest is the Deep Lens Survey (DLS) that, in a similar way to the FSVS, combines colour and variability information and explores similar variability time-scales (Becker et al. 2004). Becker et al. (2004) also provided a comprehensive review of past and ongoing variability surveys.

The future of optical variability surveys looks quite promising with the advent of large-aperture telescopes, such as the Large-aperture Synoptic Survey 8.4-m Telescope (Tyson 2002), the 4-m telescope VISTA and the 2.5-m VLT Survey Telescope.

2 OBSERVATIONS

The full FSVS data set consists of 78 Wide Field Camera (WFC) fields taken with the Isaac Newton Telescope (INT) at La Palma. The FSVS covers an area in the sky of $\sim$21 deg^2, located at mid and high Galactic latitudes ($-40 < b < -21, 15 < b < 50, 89 < b < 90$). The WFC is a mosaic of four 2k×4k CCDs. For each field, we took one set of *B*-, *I*- and *V*-band observations on a given photometric night. Photometric variability observations were taken with the *V* filter on several consecutive nights. On average, fields were observed 10–20 times within one week in the *V* band. Exposure times were 10 min with a dead time between observations of 2 min. This observing pattern allows us to sample periodicity time-scales from 2× (observing time + dead time) (i.e. 24 min) to twice the maximum time-separation of observations (which ranges from 3 to 13 d). See Groot et al. (2003) for more details.

All fields were re-observed years later to determine proper motions. In this paper, we concentrate on the shorter time-scale variability (from 0.4 h to a few days) of the targets and we do not include those observations.

Of the 78 fields, 10 were only observed in the *V* band on two or three occasions due to bad weather, making it impossible to use these for precise variability studies. We also encountered data-acquisition/reduction problems in several occasions which resulted in parts of fields being lost. Initially, 79 fields were defined but one, field 67, was never observed. For data-handling consistency, we have kept the original numbering.

A complimentary analysis on the variability at short and long time-scales (including year-long time-scales) of the FSVS has been carried out by Huber, Everett & Howell (2006). They made use of a variability test similar to that described in Section 3.1 to find signatures of the presence of variability with some indication of its time-scale and amplitude. By using the yearly re-observations, they found a variability fraction of 5–8 per cent in two survey regions. This number is larger than that found in Section 4.1 due to several factors: in our analysis we are only considering short-period variables and thus do not make use of the yearly re-observations, we determine the variability fraction using the entire area of the survey instead of two separate regions, and we use a reduced weighted χ^2 to establish variability instead of the reduced unweighted χ^2 found in the public release FSVS data products. Most of the variable sources found by Huber et al. (2006) are long-period variables classified as such, thanks to the *V* brightness of the re-observation a year later. The number of possible periodicities in the data when the sampling is sparse and the time-span long is very large and their analysis is devised to find possible variable systems more than to find their actual variability time-scale and amplitude, which is one of the main goals of the work presented here.

Table 1 gives a list of the number of times each field was observed in *V* and the maximum time-span of the data in each case. In summary, we have photometric data that can be used for variability analysis for $\sim$17.5 deg^2 out of the 21 deg^2 that constitute the FSVS. For $\sim$9.2 deg^2, the number of measurements is equal or more than 15, whereas for the other $\sim$8.3 deg^2 the number is between five and 15. This makes a difference in the accuracy with which we can measure the variability time-scale of each object.

The methods used to study the variability in the data are presented in Section 3. The results from the variability analysis are discussed in the different subsections of Section 4. In this paper, we carry out a full variability study for point sources that have not only more than four *V*-band measurements taken over a two-week baseline, but also positive detections in the *B* and *I* bands. Possible extreme colour systems are discussed in detail in Section 4.7.

2.1 Data-quality checks

We carried out several tests to check the quality of the photometry. These included plotting several quantities obtained from the data to check for anomalies. We explored how the number of detected point sources changed with epoch for each field, the average point source *V* magnitude per epoch per field and the ratio between the point source mean magnitude and the limiting magnitude for each measurement.

We identified several fields that showed anomalies, such as field 31 CCD 4, in which one of the observations (number 14) resulted in *V*-band magnitudes that were lower than the rest by 2 magnitudes. We found that the best way to identify these anomalies consisted of plotting the *V*-band magnitudes for each point source detected in each field versus its error, for each observation. An example of this test is shown in Fig. 1 where the point sources found in Field 31 CCD 4 on four different epochs are plotted. Each panel presents the test for one observation. The average *V*-band magnitude ($V_{\rm ave}$) for all point sources and the limiting *V*-band magnitude ($V_{\rm lim}$) for each image are also given. When the field was observed through thin clouds (e.g. epoch 13), the values of $V_{\rm lim}$ and $V_{\rm ave}$ decrease, but the shape of the curve does not change. On the other hand, if something went wrong with the image or the data reduction, we expect the shape of the curve to change (e.g. epoch 14) giving us an indication that we should be wary of this *V* point when doing our variability searches. We could not trace the reason for the

Table 1. Journal of observations. The number of V-band observations taken for each field, not counting those taken about a year later for proper motion studies, as well as the maximum time-interval covered in days, Δt, are given. For field 48, the two V-band measurements were taken more than a year apart. For field 51, two measurements were lost in one of the CCDs. The fraction of variable sources (FV) $\times$ 100 per field found using the χ^2 test is also given. This will be discussed in detail in Sections 3.1 and 4.1. Note that the fraction of variables found in fields 36 and 48 is very high compared to the rest of the fields. These fields were only observed in two occasions, so their variability χ^2 was calculated based only on two points. This is also the case for fields 35 and 41–45, but they do not show a fraction of variables as large. These six fields contain about twice the number of stars compared to fields 36 and 48.

Field	Number of V-band observations	Δt	FV	Field	Number of V-band observations	Δt	FV
01	10	5.07	0.59	40	9	3.07	3.44
02	11	5.07	1.04	41	2	0.06	3.22
03	13	5.11	0.21	42	2	0.91	3.91
04	12	3.04	1.19	43	2	0.03	1.62
05	12	3.09	0.55	44	2	0.03	2.05
06	10	3.11	0.74	45	2	0.03	1.90
07	10	5.99	0.48	46	19	4.18	1.06
08	11	5.07	0.09	47	5	6.97	4.20
09	10	5.02	0.79	48	2	-	8.60
10	10	3.02	0.09	49	3	5.94	5.26
11	7	3.04	0.23	50	3	6.07	3.75
12	8	3.07	0.31	51	5, 3	5.92	2.09
13	9	5.06	0.77	52	26	5.17	0.80
14	10	5.03	0.54	53	20	6.10	0.24
15	8	3.03	0.55	54	20	6.01	0.15
16	12	3.06	0.51	55	20	5.98	1.11
17	8	3.09	0.64	56	19	4.18	0.37
18	9	5.06	0.67	57	18	5.24	1.30
19	11	4.02	0.35	58	15	4.18	0.70
20	11	4.04	0.11	59	20	5.12	0.60
21	11	4.07	0.74	60	22	4.16	1.93
22	11	4.05	2.73	61	20	4.09	0.47
23	11	4.08	3.06	62	19	4.06	1.95
24	10	4.11	1.62	63	22	6.09	0.52
25	30	6.12	0.06	64	22	6.06	0.43
26	29	5.00	0.58	65	20	6.03	0.40
27	14	6.01	0.25	66	21	6.00	0.41
28	14	5.99	0.66	68	28	12.07	1.11
29	14	6.02	0.45	69	29	13.00	1.50
30	16	4.99	1.60	70	24	6.03	0.88
31	16	4.99	0.87	71	27	6.00	1.04
32	16	4.99	0.36	72	26	6.11	0.50
33	18	6.10	0.18	73	27	6.09	0.66
34	17	6.07	0.42	74	26	6.05	0.23
35	2	0.03	1.83	75	25	6.00	0.21
36	2	0.97	13.68	76	33	7.03	0.37
37	10	4.08	0.35	77	33	7.06	0.48
38	9	4.05	0.73	78	33	7.15	0.48
39	9	3.09	0.77	79	31	7.15	0.28

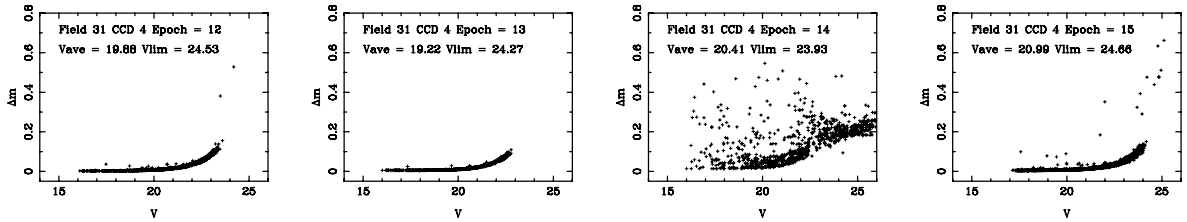

Figure 1. V magnitude versus V error for each point source detected in field 31 CCD 4 in four different epochs. These plots were generated for all fields to check the quality of the data. See the text for details.

anomaly found in epoch 14 of field 31 and just discarded this data point.

We also carried out a visual inspection of the raw unfolded light curves for all the variable point sources to identify possible problematic photometry points and when confirmed these points were thrown out.

3 VARIABILITY-ANALYSIS METHODS

3.1 The variability χ^2 test

Groot et al. (2003) determined the variability of a given point source in the FSVS by calculating the reduced χ^2 value of the object's

individual brightness measurements with respect to its weighted mean brightness value. An object is tagged as variable if its reduced χ^2 is above the 5σ level. This definition will be used in Section 4.1 to determine the fraction of variable objects in the survey. Because we have colour information for the majority of the objects, we can determine this ratio for different types of systems.

3.2 The floating mean periodogram

If we not only want to know whether an object is variable or not, but also what the time-scale and amplitude of its variability are, and thus what type of object it might be, we need to use more refined methods to determine its variability. Because of the relatively small number of V-band observations (between two and 33 depending on the field), we use the 'floating mean' periodogram technique to estimate the characteristic variability time-scale in each case. This method works better than the traditional Lomb–Scargle algorithm (Lomb 1976; Scargle 1982) for small number of points and has been successfully applied to planet searches (Cumming, Marcy & Butler 1999), and to determine the orbits of subdwarf B binaries (Morales-Rueda et al. 2003). A minimum number of five V measurements are required to calculate the floating mean periodogram.

The floating mean periodogram consists of fitting the data with a model composed of a sinusoid plus a constant of the form

$$A(t) = \gamma + K \sin\left[\frac{2\pi(t - t_0)}{P}\right],$$

where γ is the average V magnitude, K is the amplitude of the V variability, P is the period and t is the time of observation. For each given period, we perform singular value decomposition least-squares fitting of the data, solving for γ and K (Press et al. 1992). We obtain the χ^2 of the fits as a function of frequency $f = 1/P$ and select the minima of this χ^2 function.

To test whether the periodogram was able to recover the correct periods, we generated, for at least nine different amplitudes per field, synthetic light curves that vary sinusoidally with periods between 24 min and several days (we chose the upper limit to be twice the time-span of the observations) in period steps of 0.1 d, using the time-sampling of each field. For each amplitude and period, we generated light curves with 20 different phasings, that is, 20 different values of t_0. For each of these 20 phasings, we generated 10 light curves where the magnitude for each point was calculated, given the period, the phasing, the amplitude and a fixed average magnitude. An error was added to the resulting magnitude for each point. This error was calculated by drawing a random number from a normal distribution centred on zero with standard deviation of 0.03, which is the average V-band error found in the FSVS data.

We then used the floating mean periodogram to calculate the most probable period for each light curve, averaging the periods obtained for the 200 different light curves generated for each input time-scale and amplitude. The average obtained was a weighted average where the weights used were the errors of the periods determined. We stopped the period search when the difference between the true and the calculated period was larger than 3σ. This condition was always reached before we got to the maximum period allowed in the search. We noted large deviations (although still within the 3σ difference) between the calculated and true values at certain isolated periods. In these cases, the true value for the following periods was again successfully recovered. These deviations are caused by the sampling windows of each given field. The presence of these isolated deviations prompted us to select the criteria described above to stop the simulated light curve fitting even when, in occasions, the errors on the calculated period were so large as to render the period determination highly inaccurate. To account for this inaccuracy, we will apply further filtering criteria to the errors of the periods determined from the data in Section 4.3.

After carrying out the simulations, the result for each field, or at least for the ones with more than 10 observations, is that true periods are recovered successfully with an error that increases with period. A few fields also show small deviations (but still within 3σ) from the true values at the shortest period (24 min). A common trend we observe is that, as we are reaching the limit period, the calculated values tend to underestimate the true periods at the same time that the error in the calculated period increases. This is clear in both panels of Fig. 2 where we have plotted the calculated period versus the true period. This seems to indicate that, when pushed to the limit, the periods calculated by the floating mean periodogram will be shorter than the true ones. Fig. 2 shows, as an illustration, two example graphs for two fields that have a very different number of observations, field 47 with only five V-band observations and field 78 with 33 observations. Note that not only the number of observations is of importance, but that using a different time-sampling also generates slightly different graphs even with the same number of observations. The amplitude of the variability assumed also influences indirectly the maximum period we can determine in each case. Specifically, it is the ratio between the amplitude of the variability and the errors in the photometry which influences the success in recovering a period. By fixing the photometric errors in the simulations to

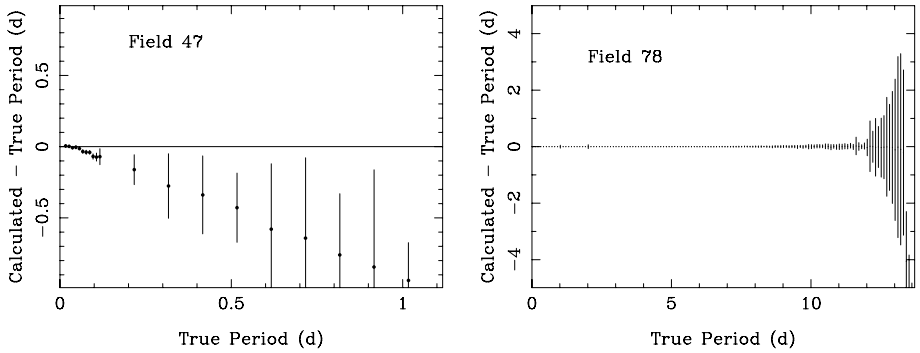

Figure 2. True period versus calculated true period, using the floating mean periodogram for two example fields, field 47 with five V-band measurements and field 78 with 33 measurements. The period search was stopped when either the difference between the calculated and the true period was larger than three times the error in the period, or the maximum searchable period was reached, that is, two times the time-baseline (although this last condition was never reached). The ratio of the amplitude of the variability to error assumed in both examples is 50.

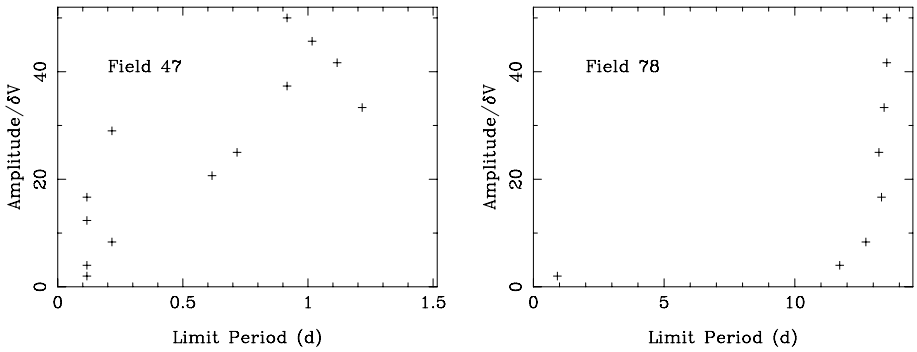

Figure 3. Maximum period that can be reconstructed from the simulated data depending on the ratio of the amplitude of the variability to the error in $V(\delta V)$. The period search was stopped when the same conditions described in Fig. 2 were reached. The period search was carried out fixing the error in V to 0.03 mag and changing the amplitude of the variability. This is the average error in brightness we find in the FSVS.

$\sigma_{\text{average}} = 0.03$ mag, we explore the influence of this ratio by varying only the amplitude of the variability. The graphs in Fig. 2 have been obtained assuming a variability amplitude of 1.5 mag (the maximum value used in the simulations) equivalent to an amplitude – V-band error ratio of 50.

We obtain similar curves for all the fields to determine how effective the algorithm is at finding the true periods depending not only on the sampling and the number of observations, but also on the amplitude of the variability and the brightness of the objects (which define the errors in the V-band magnitudes). For each field, we generate a curve like those shown in Fig. 3, which present the maximum period that we can reconstruct from the simulated data for a range of variability amplitudes. As expected, the larger the amplitude of the variability (equivalent to a larger amplitude–error ratio), the longer the time-scale of the variability that we can detect. The sampling and the time-span of the observations have a direct influence on the maximum period we can detect. The graphs are presented only for the two example fields, 47 and 78, where the number of V-band observations is very different over the same time-span, ∼7 d. In the case of field 47, with only five measurements, the maximum period we can reconstruct before the difference between true and calculated periods is larger than 3σ is about 0.4 d (see left-hand panel of Fig. 2). Its limit period graph (left-hand panel of Fig. 3) shows some departures from the expected behaviour, that is, higher limit period as the amplitude–error ratio increases. In contrast, for field 78, with 33 V measurements we can detect periods of up to 13.5 d for the same variability amplitude and the limit period graph shows the expected behaviour. A similar number of measurements over a shorter time-span will only allow us to measure shorter variability time-scales. For example, for field 26, with 29 measurements over 5 d, the maximum period we can reconstruct (for variability amplitude of 1.5 mag) is 9.3 d.

We want to recall at this point, that by using the floating mean periodogram we are fitting the data with sinusoidal curves. Any non-sinusoidal, or indeed any non-periodic variability present in the data will be poorly fitted.

The maximum period that can be reconstructed for all the fields in the FSVS simultaneously is plotted in Fig. 4. For an amplitude of the variability of ∼0.25 mag (equivalent to an amplitude to magnitude error ratio of ∼8.3), we can reconstruct variability periods of up to 1 d for ∼17.58 deg^2 out of the 18.11 deg^2 available for search (66 fields out of the 68 with more than four V-band measurements); we can reconstruct variabilities of up to 5 d for ∼13.31 deg^2 (50 fields). For amplitudes of 1.5 mag (amplitude to magnitude error ratio of 50), we can reconstruct periods of up to 11 d for a region of 6.66 deg^2 (25 fields) and so on. We can only search for periods of the order of 20 d in two fields.

We are also interested in detecting small-amplitude and short-period variability; the limits of the data being a 24-min sampling and the photometric accuracy of ∼3 mmag for the brightest objects (Groot et al. 2003). The right-hand panel of Fig. 4 zooms into the the short time-scale, small-amplitude variability region. We reconstruct successfully (i.e. with less than a 3σ difference between the true and calculated periods) the minimum searchable period in all fields.

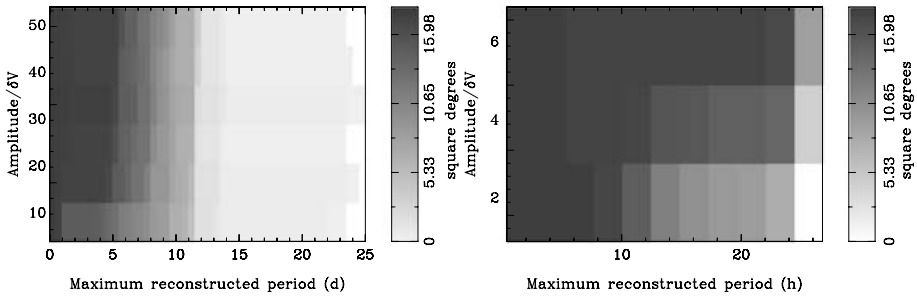

Figure 4. Left-hand panel: grey-scale map presenting the number of deg^2 in the sky for which we can reconstruct a given variability time-scale depending on the ratio of the variability amplitude to the magnitude error. Note that if a variability scale of 5 d can be reconstructed for a given field, then also variabilities smaller than 5 d can be reconstructed. The minimum limit being the minimum possible searchable period of 24 min. Right-hand panel: same information but zooming into the short-period, small-amplitude/error region. We reconstruct the minimum searchable period for all fields. Note that the structure seen on this panel cannot be seen on the left-hand side panel due to the coarser binning in amplitude/δV of the left-hand side panel.

3.2.1 Our efficiency to detect the variability time-scales of some interesting astronomical objects

Some interesting astronomical objects, such as cataclysmic variables (CVs) and RR Lyr show characteristic variability time-scales. CV periods range from 80 min to ∼6 h (although some of them show longer orbital periods, such as GK Per, with a 2-d orbit). The variability of RR Lyrae ranges from ∼6 h to about 1 d. Other interesting systems, such as AM CVn binaries, show orbital periods of the order of tens of minutes, too short to be detected in the FSVS. On the other hand, orbital periods of 80 min will be detected in the full area of the FSVS, as long as the ratio of the amplitude of the variability to the error in the V magnitude is at least 10, that is, we would be able to detect all 80-min variables down to $V = 24$ if their variability amplitude is at least 2 mag, down to $V = 23$ if the variability amplitude is at least 0.7 mag, and down to $V = 22$ if the variability amplitude is at least 0.36 mag. CVs show characteristic orbital variability amplitudes of the order of 0.1–0.4 mag; thus, we will be able to detect a fraction at least down to $V = 22$. For certain fields, when looking at the short-period region, the calculated period underestimates the value of the true period. This will most probably happen also for the real light curves.

Orbital periods of up to 6 h, and between 6 h and 1 d (this last period range is typical of RR Lyr) will be detected in 17.58 deg^2 (all fields but two) as long as the ratio of the amplitude of the variability to the V error is at least 20, that is, we would be able to detect all variables with periods of up to 1 d in this area down to $V = 24$ if the variability amplitude is larger than 4 mag, and down to $V = 23$ if the variability amplitude is at least 1.4 mag. The variability amplitudes, typical of RR Lyr, range between ∼0.5 and >1 mag, which indicates that we are sensitive to RR Lyr down to $V = 23$ as long as the variability amplitude is at least ∼1.4 mag.

Other pulsating stars, such as γ Doradus stars, δ Scuti stars, slowly pulsating B stars, β Cep stars and short-period Cepheids show pulsation periods and amplitudes in the detectable range of this survey. Some of them, like δ Scuti stars, show very complicated oscillation patterns that are far from sinusoidal which means that, although they would be detected as variables with the χ^2 test, the periods reconstructed with the floating mean periodogram will most probably be incorrect. Short-period pulsators, such as rapidly oscillating Ap stars, PG1159 stars, pulsating subdwarf B stars and pulsating white dwarfs, and long-period pulsators, such as RV Tauri stars and Mira stars, will not be detected in the FSVS as their pulsating periods lie outside the range we are sensitive to. Solar-like stars show very small amplitude pulsations that cannot be detected in the FSVS.

Asteroids show rotational periods of the order of a few hours and also lie in the detectable range of the FSVS. We see a number of asteroid tracks in the FSVS images but these asteroids do not stay in the same position from image to image and are discarded during data reduction.

We will use these results again in Section 4.3 to estimate how reliable our detections and non-detections for variability are at given time-scales and amplitudes.

4 RESULTS

4.1 Fraction of variable sources

In the entire FSVS, using the χ^2 test, after discarding problematic points, we find a total of 1713 short time-scale variable V-band point sources that have been detected also in the B and I bands. The number of non-variable sources found (after applying the same criteria as for the variable sources, that is, accounting for problematic points and positive detections in B and I) is 173 276 (∼1 per cent of all point sources detected are short-term variables).

In the top left-hand panel of Fig. 5, we present the distribution of sources in the FSVS in the form of a grey-scale plot, which shows that most objects fall along the main sequence with the largest numbers at its blue end. The top right-hand panel presents the same plot for the variable sources in the FSVS, as determined by the χ^2

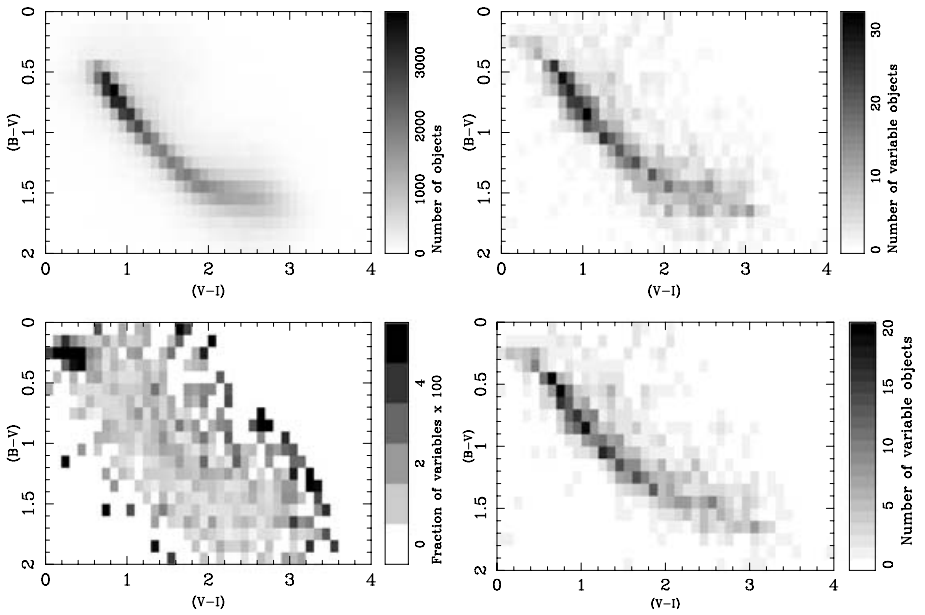

Figure 5. Top left-hand panel: non-variable sources in the FSVS. Top right-hand panel: short-term variable sources in the FSVS. Bottom left-hand panel: fraction of short-term variable sources in the FSVS. The fraction is presented in percentages. The region in the colour–colour diagram where there are more variable sources lies above the blue cut-off, that is, $(B - V) < 0.38$ and $0 < (V - I) < 1$. Bottom right-hand panel: colour–colour diagram presenting the 976 variable point sources that have more than four measurements and can be studied using the floating mean periodogram method. Note that some of the blue variables found in this diagram might be quasi-stellar objects.

test. Again, most sources are situated along the main sequence, but there are also a significant fraction of sources above the main sequence and as a 'blue' extension of the main sequence. To highlight the difference in distribution between the variable and non-variable sources, we present the fraction of variable sources as a function of colour in the lower left-hand panel (which is basically the ratio of the upper two panels in Fig. 5). This shows a clear enhancement of sources above the blue tip of the main sequence (about 4 per cent are variables) and a less-marked enhancement to the right-hand side and above the main sequence, while the main sequence itself appears as an area with relatively few variables, of the order of 1 per cent. These values agree with those found by Everett et al. (2002) in a similar, albeit shallower, study.

The fraction of variable point sources found in each field using the χ^2 test is given in Table 1. The fraction of variables differs from field to field ranging from 0.06 to 13.68 per cent. We find that fields with less than four measurements tend to have larger fractions of variables, but we are not certain that there is a direct correlation with the number of observations and that other effects, such as position in the sky, are not taking place. If we do not consider the fields with less than four observations, we determine a 0.7 per cent fraction of variables in the full FSVS. The distribution along the main sequence decreases only slightly, by 0.2 per cent, for all colour–colour bins.

4.2 Sample of variables studied with the floating mean periodogram

10 fields have less than five V measurements. The time-scale of the variability for the variables in these 10 fields cannot be determined because of the low number of measurements; thus, only a fraction of the 1713 short-term variables found in the FSVS can be studied in more detail using the floating mean periodogram. Once we account for fields with less than five measurements, for problematic epochs, and for objects that were observed more than four times but were only detected four times or less, we end up with 976 point sources that can be studied in further detail. In most cases, the non-detection of a source was the result of faint objects, occasionally falling below the limit of detection, and in some cases of the objects being blended or truncated. After accounting for these three factors, we find that the fraction of variable systems found is independent of the number of V measurements. For the objects with more than four detections, information about the time-scale and amplitude of the variability can be obtained. The distribution of these 976 sources in the colour–colour diagram is given in the bottom right-hand panel of Fig. 5.

4.3 Time-scale and amplitude of the variability

When we run the floating mean periodogram on the real data light curves, we obtain their most likely variability time-scale and the amplitude of the variability on that time-scale. After rejecting those sources for which the period and amplitude measured lie outside the ranges that can be reconstructed, according to the simulations carried out in Section 3.2, we are left with 744 variable point sources out of the 976 mentioned above.

To understand this sample of variables, we select different cut-offs for the error in the variability time-scale and amplitude calculated. Table 2 gives the fraction of variable point sources found for different combinations of error cut-offs in time-scale and amplitude. Applying an error cut-off of 30 per cent in the periods and 50 per cent in the amplitudes, we can already reconstruct the 744 initial variables. Applying an error cut-off of 30 per cent in both period and amplitude, we find that 50 per cent of the variables show periods between 24 min and 6 h, 22 per cent between 6 h and 1 d, 20 per cent between 1 and 4 d, and 8 per cent show periods above 4 d. If we apply fairly strict error cut-offs for the period and amplitudes, that is, 10 per cent, the number of variable sources decreases to 219, of which the distribution in the same period bins is 51, 20, 19 and 10 per cent, respectively.

Table 2. The fraction of variable objects (out of the 744) found in the FSVS for different cut-off limits on the error of the time-scale and the error of the amplitude.

δP (per cent)	10	20	30	40
δA (per cent)				
10	29.4	29.7	29.7	29.7
20	75.7	76.2	76.3	76.3
30	91.4	92.2	92.6	92.6
40	96.6	97.4	97.8	97.8

If we assume a normal distribution for the data, a 50 per cent error corresponds to 2σ, a 30 per cent error to 3.3σ, a 20 per cent to 5σ, and a 10 per cent to 10σ.

The number of variable point sources for which we can determine their variability time-scales and amplitudes by using the floating mean periodogram test is a very good fraction of the total number of variables detected using the χ^2 test (i.e. $\sim$700 out of the 976 if we use error cut-offs of the order of 30 per cent).

Fig. 6 shows the ratio of variable sources for which we have determined the time-scale and the amplitude of their variability with an error less than 20 per cent with the floating mean periodogram with respect to the number of sources flagged as variable with the χ^2 test as a function of the number of observations. To account for the fact that there are large differences between the number of variable sources for each field, we have only plotted those fields for which the number of variable sources is 10 or more. There is a clear correlation between the number of observations and the fraction of variables we can solve with the floating mean periodogram. Including

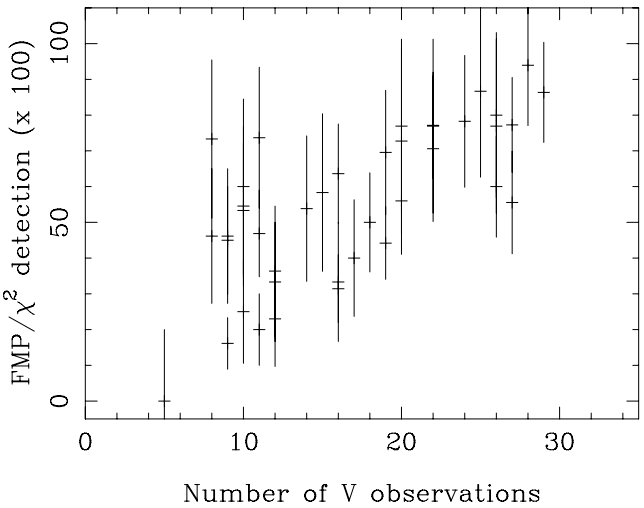

Figure 6. Ratio of variable sources solved with the floating mean periodogram with respect to the number of sources flagged as variables with the χ^2 test, as a function of the number of observations. We have only included the sources determined using the floating mean periodogram that have errors of less than 20 per cent. We only plot those fields that contain more than 10 variables. FMP stands for floating mean periodogram.

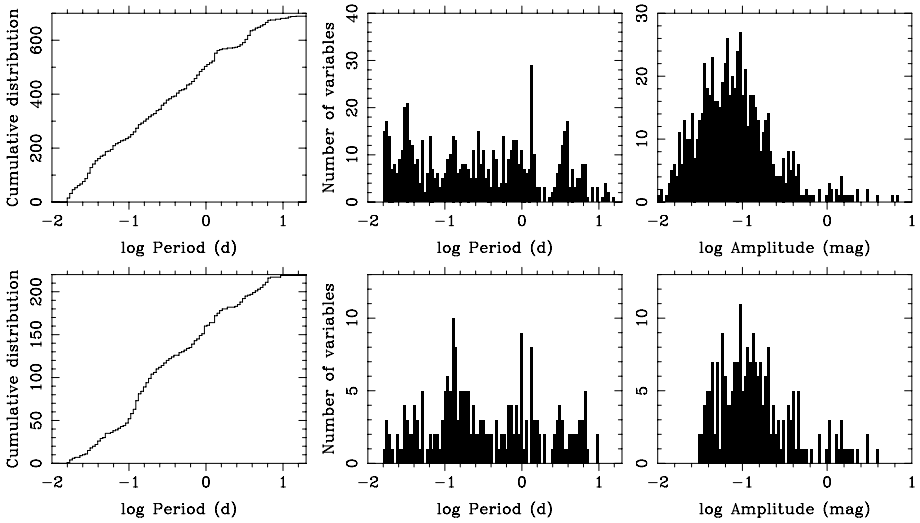

Figure 7. Histograms showing the cumulative period distribution (left-hand panels), the period distribution (middle panels) and the amplitude distribution (right-hand panels) for the short-term variable point sources in the FSVS. Top panels: the 689 out of 744 sources with accuracies in the periods and amplitudes of the order of 30 per cent or less. Bottom panels: sources where the error in their periods and amplitudes is of the order of 10 per cent or less.

the fields with less than 10 variables increases the scatter in the plot, whereas including only those fields with 20 or more variables decreases the scatter. The slope of the correlation remains the same and indicates that with a number of observations of the order of 30, taken within a two-week time-span, we can reconstruct most variables present in the data (with those periods and amplitudes in the range determined in Section 3.2). Of course, this argument assumes that the light curves of the variables are close to sinusoidal.

Fig. 7 presents the distribution of variables we find in the FSVS according to the period and amplitude of the variability as well as their cumulative period distribution. The top panels consider the total number of variables in the trusted range of periods and amplitudes (689) where the error on the periods and amplitudes is less than 30 per cent. The bottom panels present the distributions when we only take the systems where the period and amplitude determined have a maximum error of 10 per cent. In both cases, we find that most systems lie at short periods and low amplitudes, with only a few systems showing larger amplitudes and periods. We find that 50 per cent of the objects show periods below 6 h with peaks in the 30 per cent error distribution at ∼24 min, ∼0.03 d (∼43 min), ∼0.12 d (∼2.9 h), ∼0.79 d (∼19 h), ∼1.3 d and ∼4 d, and in the 10 per cent distribution at ∼0.12 d (∼2.9 h). In the 30 per cent period distribution, the clump of sources between ∼24 and 36 min ($-1.778 < \log P < -1.6$) contains 67 sources. To confirm that these are short-period variables, and not just a systematic problem caused by the sampling (after all the minimum period we are sensitive to is 24 min), they were inspected by eye resulting in 80 per cent being bona fide short-period variables with the remaining 20 per cent showing only one point off the average brightness of the target and thus giving the short-period result based only on one-point variability. These one-point-off sources are not present in the 10 per cent sample.

Regarding the amplitude distribution, 50 per cent of the objects show amplitudes lower than ∼0.07 mag in the 30 per cent error sample and lower than ∼0.12 mag in the 10 per cent sample.

When we combine the number of sources we find per period and amplitude bin with the sensitivity of the floating mean periodogram search, plotted in Fig. 4, we obtain lower limits for the space density of variables, that is, the number of variables per deg^2, versus period.

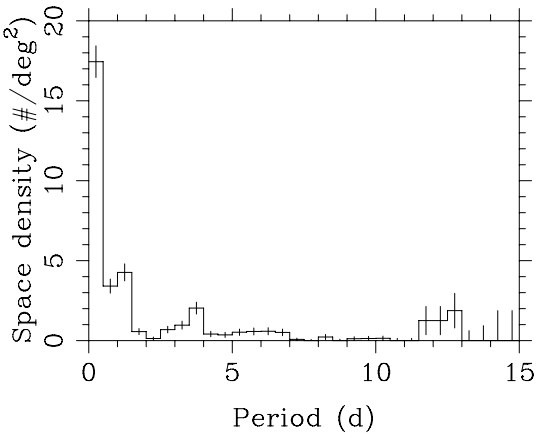

Figure 8. Space density of variables obtained from the FSVS.

These are presented in the form of a histogram in Fig. 8. We see four distinct peaks in the distribution centred on 6 h, 1 d, 3.75 and 12.75 d with a somewhat less-significant peak at 6 d. The highest densities of variables show periods below 12 h. These periods include CVs, RR Lyr stars, and other short-period pulsators, such as δ Scuti stars. The period range centred on 1 d includes also possible CVs, RR Lyr and other pulsators, like γ Doradus stars and Population II Cepheids. At 3.75 d, we would still find some longer-period CVs, γ Doradus stars, Population II Cepheids and longer-period pulsators, such as subdwarf B stars. At periods around 12.75 d, we expect to find, apart from binaries with those orbital periods, Population II Cepheids contributing to the space density of variables.

4.4 Variability colour–colour diagrams

Keeping in mind the uncertainty of the variability time-scales determined, when we combine the variability information with the colour information available for the FSVS, we obtain the colour–colour diagrams shown in Fig. 9. We find that, if we take only the sources with less than 30 per cent errors in their time-scales and the amplitudes, 344 point sources show variabilities shorter than 6 h

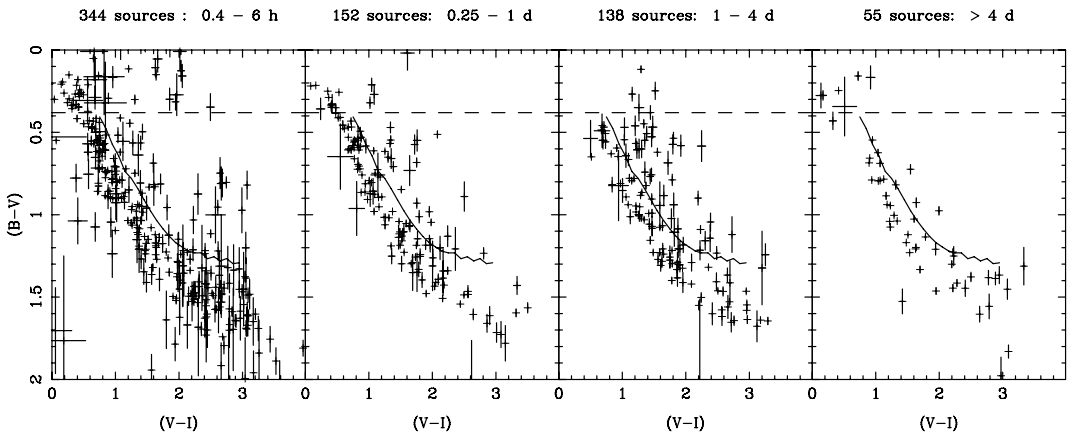

Figure 9. Colour–colour diagrams for several variability time-scales obtained from the FSVS after applying a 30 per cent error cut-off in both the time-scale and amplitude of the variability. The solid curve indicates the 3σ upper limit of the main sequence. The dashed line indicates the blue cut-off at $(B-V) < 0.38$.

(0.25 d). These short time-scale variables are found along the main sequence in the colour–colour diagram (see first panel of Fig. 9), where we expect to find, for example, δ Scuti stars, as well as above the main sequence and in more extreme colour areas usually filled by binary systems where one of the components is blue and the other red, for example, detached red dwarf–white dwarf binaries. At these short time-scale variabilities, we also find a clump of objects above the, so-called, blue cut-off at $(B-V) < 0.38$. The blue cut-off of the main sequence results from the combination of the number density of different spectral types and the scaleheight of the Galaxy. The colours and the short variability time-scales, of the order of characteristic close binary orbital periods, suggest that these sources above the blue cut-off are possibly interacting binary systems of the CV type or detached binary systems, such as subdwarf B binaries. Longer-coverage, better-sampled light curves combined with spectroscopy are necessary in order to identify the sources.

The variable sources with time-scales shorter than 6 h represent 50 per cent of the total number of short time-scale variables in the survey. Fig. 10 shows how most of those short-period sources subdivide in smaller variability time-scale ranges. We find that about half of the short-period sources have variability time-scales shorter than 1 h. These are again distributed along the main sequence with a few objects placed above it.

There are 152 objects showing variability in the 0.25–1 d range. These objects are also mostly distributed along the main sequence, including γ Doradus pulsators amongst others, with some cases found in the extreme colour region. The RR Lyr variables present in the survey should be found in this variability range. If we combine this with the colours expected for RR Lyr systems, that is, $0.1 < (B-V) < 0.45, 0.1 < (V-I) < 0.65$ (Guldenschuh et al. 2005), we find 12 RR Lyr candidates. One of these will be discussed, as an example, in Section 4.6.

We find 138 sources that show variabilities between 1 and 4 d, again distributed mostly along the main sequence. This would include γ Doradus pulsators as well as Population II Cepheids. There are 55 point sources that show variabilities on time-scales longer than 4 d. Binary systems with these periods, as well as Population II Cepheids are included in this period range. The blue sources found in these two period ranges above the blue cut-off could be subdwarf B slow pulsators or binaries.

Fig. 11 presents similar diagrams to those in Fig. 9 but for the sources where the error limits were set to 20 per cent. The distribution of variables in the diagrams is very similar to the initial one. Again about half of the sources show variability time-scales shorter than 6 h. Most of the objects that have disappeared from the diagram come from the shorter period ranges (23 per cent out of the 0.4–6 h bin and 22 per cent out of the 0.25–1 d bin). This could be due to the fact that if the signal is not sinusoidal or regular, the floating mean periodogram tends to calculate periods shorter than the input ones with large errors. It is worth noting

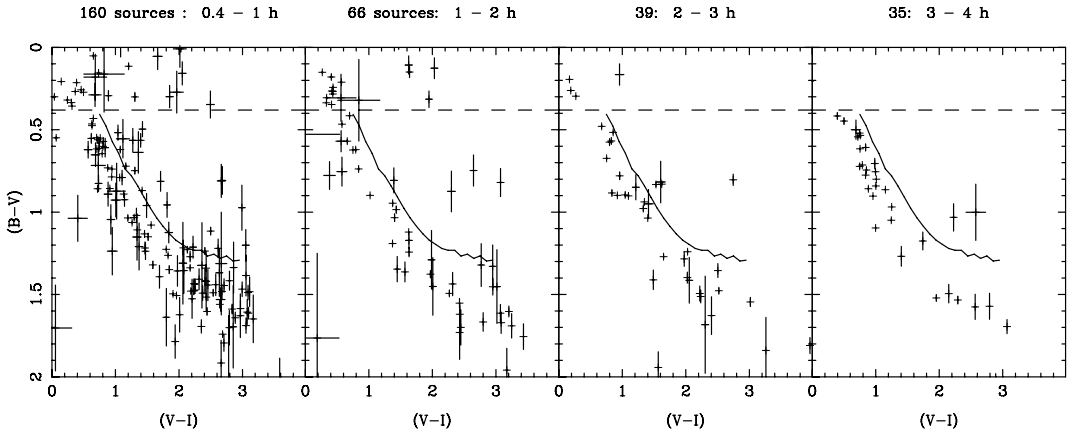

Figure 10. Same as in Fig. 9 but only for short variability time-scales. Most short-period variables show variability time-scales lower than 1 h.

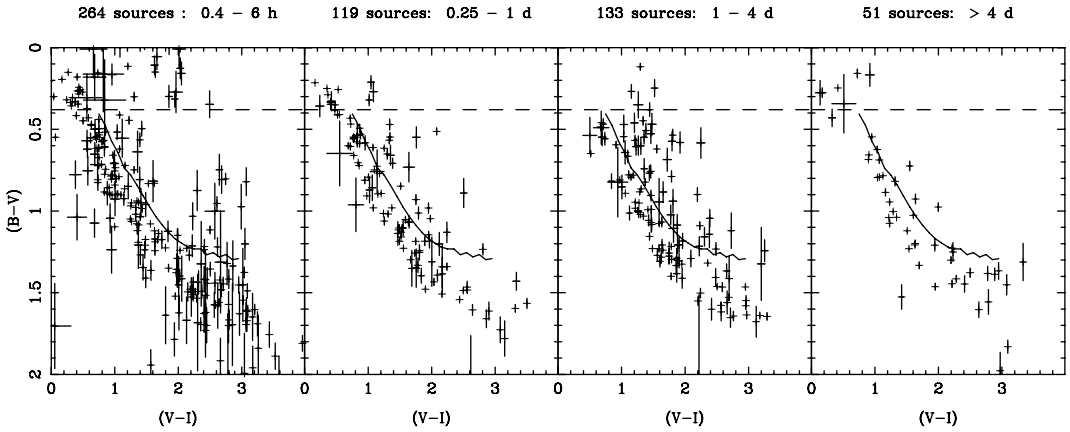

Figure 11. Same as in Fig. 9 but with error limits set to 20 for both time-scales and amplitudes.

that a few of the interesting objects above the blue cut-off have disappeared.

4.5 Fraction of variable sources as a function of spectral type

The fraction of variable point sources along the main sequence, as a function of spectral type (as defined in Johnson 1966), is presented in Table 3. The number of variables used here is that obtained from the χ^2 test. The fraction of variables is constant with spectral type and has a value around 1 per cent.

We also present the distribution of variability periods and amplitudes measured for the number of variables that were analysed with the floating mean periodogram algorithm. Four period bins and four amplitude bins are presented in Table 4. Some spectral-type ranges contain very few objects. For those with a larger number of objects (K0–M5), the variable sources spread themselves in similar fractions in the spectra ranges K0–M0 with more short-period systems in the spectral range M0–M5. The fraction of variables with time-scales longer than 4 d is significantly smaller than that in the other time-scale bins. In the case of the amplitudes of the

Table 3. The fraction of variable sources per spectral-type bin found in the FSVS. Note that although the first main-sequence bin (spectral types F0–F5) contains more variables than the rest, this is likely to be the result of including non-main-sequence sources in that bin. Non-MS stands for non-main-sequence sources.

Spectral type	$B-V$	$V-I$	# Var	# Sources	Fraction (per cent)
Non-MS	<0.38	0.47–0.64	11	700	1.6
Non-MS	<0.38	0.00–0.4	29	833	3.5
F0–F5	0.31–0.43	0.47–0.64	13	602	2.2
F5–G0	0.43–0.59	0.64–0.81	62	6054	1.0
G0–G5	0.59–0.66	0.81–0.89	20	1816	1.1
G5–K0	0.66–0.82	0.89–1.06	63	6814	0.9
K0–K5	0.82–1.15	1.06–1.62	204	20 207	1.0
K5–M0	1.15–1.41	1.62–2.19	133	12 974	1.0
M0–M5	1.41–1.61	2.19–3.47	153	16 256	0.95
M5–M8	1.61–2.00	3.47–4.70	3	179	1.7

Table 4. Period and amplitude distributions of the main-sequence variables analysed with the floating mean periodogram. Four bins for the variability time-scale and four for the variability amplitude are shown. The percentage of sources in each bin is given. FMP stands for floating mean periodogram. Amplitudes are given in magnitudes.

Spectral type	# VarFMP	Period distribution (per cent)				Amplitude distribution (per cent)			
		0.4–0.6 h	0.25–1.0 d	1.0–4.0 d	>4 d	0.01–0.1	0.1–0.25	0.25–1.0	>1.0
F0–F5	6	50.0	33.3	0	16.6	16.6	50.0	16.6	16.6
F5–G0	30	53.3	23.3	23.3	0	60	26.6	10.0	3.3
G0–G5	6	50.0	33.3	16.6	0	83.3	16.6	0	0
G5–K0	18	61.1	22.2	5.5	11.1	88.8	11.1	0	0
K0–K5	86	43.0	23.2	23.2	10.5	82.6	11.6	5.8	0
K5–M0	66	36.4	33.3	25.8	4.5	77.3	12.1	7.6	3.0
M0–M5	69	63.8	10.1	18.8	7.2	78.3	17.4	4.3	0
M5–M8	2	100.0	0	0	0	50	50	0	0

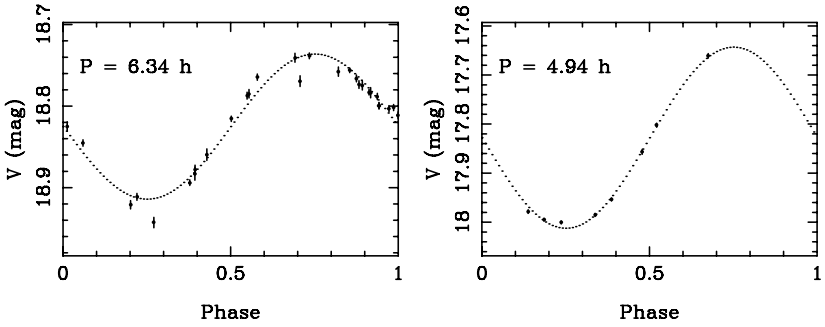

Figure 12. Light curves of two example objects folded on the period determined with the floating mean periodogram. The left-hand side light curve corresponds to one of the RR Lyr candidates discussed in Section 4.4 and the right-hand side light curve corresponds to a subdwarf B star candidate. The best sinusoidal fit is also plotted.

variability, most sources show variabilities with amplitudes lower than 0.1 mag.

4.6 Example light curves

Fig. 12 presents the light curves for two example sources found in our data. The examples have only been selected to illustrate two very different samplings. The first example corresponds to one of the candidate RR Lyr (see Section 4.4) for which we determined a period of 6.34 h from the floating mean periodogram. The second example corresponds to a source with very blue colours, for which we have obtained spectra that suggests it is a subdwarf B star. The period measured for this system, which probably corresponds to its orbital period in a binary system, is 4.95 h. For both sources, we present the measurements as a function of phase folded at the period determined from the floating mean periodogram. The best sinusoidal fit to the data is also plotted.

The FSVS covers a region in the sky in which there are two known CVs, GO Com and V394 Lyr. These two sources were identified as variables in both the χ^2 and the floating mean periodogram tests. Interestingly enough, both of them went into outburst during the observations which made it more difficult to determine their orbital periods. GO Com was observed in three different epochs and it decreased by a magnitude in V from the second to the third epoch (from 19.4 to 18.5). In an attempt to subtract the outburst contribution to the variability, and thus to be able to measure its orbital period, we calculated its average brightness for each epoch and subtracted the average from the measurements taken on that epoch. When we run the floating mean periodogram on the resulting light curve, we obtain a periodogram with two main groups of aliases, one centred on 30 min and another on 90 min. The sampling of the light curve does not allow us to determine the period with more accuracy than this. The second alias lies near the 94.8 min period determined by Howell, Szkody & Cannizzo (1995). V394 Lyr was observed in seven epochs and it decreased by two magnitudes in V from the first to the sixth (from 19.1 to 17) starting to rise on the seventh. We followed the same steps outlined above for GO Com and found the lower χ^2 aliases to be 43 min and 4.32 h. There are no measurements of the orbital period of V394 Lyr in the literature that we can compare these values with. The folded light curves on these two periods do not look convincing which leads us to think that none of these is the true orbital period of the system.

4.7 Sources not detected in all three bands

A third of the variable point sources found in the FSVS, using the χ^2 test, were not detected either in B, I or in both B and I bands. In a handful of cases, this was due to the point source being close to the CCD boundary, in 21 per cent of the cases the source appeared as blended with another one, in 28 per cent of the cases the source was not detected because it was too faint, and in 50 per cent of the cases the source was saturated in the I band. Most of these sources saturated in the I band are very bright in the three bands (71 per cent), indicating that about one-sixth of the variable sources found are at the bright end of the survey. This is expected as most variables probably show low-amplitude variations which are easier to detect for bright sources. In the case of the blended sources, blending would most probably affect the V-band magnitudes, perhaps introducing spurious variability.

On the other hand, 29 per cent of the sources undetected in B and/or I, do show larger colour differences, $(B - I) > 3$ and up to 5 mag in some cases. Colour differences of $(B - I) > 3$ are expected for some main-sequence stars and do not imply that we are dealing with extreme colour objects. The lower-limit colours calculated for these sources (by assuming their I-band magnitude to be equivalent to the I-band magnitude of the brightest unsaturated star in the field) fill an area of the colour space, which is also filled by the point sources that were detected (unsaturated) in the three bands. This indicates that, although their colours are more extreme, they are not unusual compared with the sources detected in all three bands; they are just brighter and therefore saturated in the I band.

The same analysis carried out in Section 4.3 for point sources with B, I and V detections, and more than four V measurements can be carried out for 154 sources with no B and/or I detections. In these cases, the information we have of the variable sources is only of their time-scales and amplitudes and not of their colours. Once we discard sources for which their calculated periods and amplitudes lie outside the trustable ranges determined in Section 3.2 for each field, we are left with 71 short-period variable sources. We find that 29.5 per cent of the variables with 30 per cent accuracy in their periods and amplitudes show periods between 0.4 and 6 h, 39.3 per cent between 6 h and 1 d, 21.3 per cent between 1 and 4 d, and 9.8 per cent of more than 4 d. These values are slightly different (19, 23.8, 33.3 and 23.8, respectively) if we consider the 21 sources where the periods and amplitudes determined have errors of less than 10 per cent. When we compare this distribution of variables in period bins with the one we found for systems with B and I measurements (50, 22 20, 8 per cent, respectively, for each period bin), we find that the number of shorter-period variables (first period range) is smaller for the sources with no B and/or I detections, and the number of variables in the last two period bins is larger.

5 CONCLUSIONS

We have analysed the short time-scale variability information contained in the FSVS and find that about 1 per cent of all point sources are variable. Of those variables, about 50 per cent show variability time-scales shorter than 6 h, 22 per cent show variabilities between 6 h and 1 d, 20 per cent between 1 and 4 d and 8 per cent show periods longer than 4 d. The distribution of variables with spectral type is fairly constant along the main sequence, with 1 per cent of all the sources being variable, except at the blue end of the main sequence where the fraction of variable sources increases possibly due to contamination by non-main-sequence sources. Above the main sequence, beyond the blue cut-off at $(B - V) < 0.38$, we find that the fraction of variables increases to 3.5 per cent.

The highest space densities of variables found in the FSVS (i.e. 17 deg^{-2}) show periods below 12 h. These include CVs, RR Lyr stars, and other short-period pulsators, such as δ Scuti stars. We find a density of four variables per deg^2 centred on a 1 d period which includes longer-period CVs, RR Lyr and other pulsators, like γ Doradus stars and Population II Cepheids. A space density of two variables per deg^2 at 3.75 d includes some longer-period CVs, γ Doradus stars, Population II Cepheids and longer-period pulsators, such as subdwarf B stars. At 12.75 d, we also find two variables per deg^2. These would be mainly binaries with those orbital periods and Population II Cepheids.

It is easier to compare these space densities with those expected for the mentioned populations when we combine the period information with the colours of the populations under study. The case of CVs and many pulsators is complicated as they appear mixed through several period and colour ranges and in many cases it is necessary to obtain spectra to confirm the nature of the variable source. The space densities of CVs and subdwarf B stars will be studied in detail in a future paper. In the case of RR Lyr stars, we find three certain members and nine other candidates down to $V = 21.6$. Assuming that we have detected all RR Lyr between $V = 16$ and 22, we determine a space density of $\sim 10^{-3}$ kpc^{-3} in agreement with the space density determined by Preston, Shectman & Beers (1991) at a distance of 100–150 kpc from the Galactic Centre.

By using the floating mean periodogram, we have determined the most likely periods and amplitudes of a fraction of the variables found in the FSVS. We find that we are complete down to $V = 22$ for CVs in the minimum period (80 min) as long as they show variability amplitudes of the order of 0.4 mag. We are complete down to $V = 22$ for periods between 80 min and 1 d in a 17.82-deg^2 area of the survey as long as the amplitude of the variability is at least 0.7 mag. This includes most RR Lyr stars. We will be able to detect RR Lyr also down to $V = 23$ when their variability amplitudes are at least 1.5 mag.

ACKNOWLEDGMENTS

We thank T. R. Marsh for making his analysis software available. The FSVS was supported by NWO Spinoza grant 08-0 to E. van den Heuvel. The FSVS is part of the INT Wide Field Survey. LM-R, PJG and EJMvdB are supported by NWO-VIDI grant 39.042.201 to PJG. GN is supported by NWO-VENI grant 639.041.405. The INT is operated on the island of La Palma by the Isaac Newton Group in the Spanish Observatorio del Roque de los Muchachos of the Instituto de Astrofísica de Canarias.

REFERENCES

Becker A. C. et al., 2004, ApJ, 611, 418
Brinkworth C. S., Marsh T. R., Morales-Rueda L., Maxted P. F. L., Burleigh M. R., Good S. A., 2005, MNRAS, 357, 333
Brown T. M., Gilliland R. L., 1994, ARA&A, 32, 37
Cumming A., Marcy G. W., Butler R. P., 1999, ApJ 526, 890
Everett M. E., Howell S. B., van Belle G. T., Ciardi D. R., 2002, PASP, 114, 656
Groot P. J. et al., 2003, MNRAS, 339, 427
Guldenschuh K. A. et al., 2005, PASP, 117, 721
Howell S. B., Szkody P., Cannizzo J. K., 1995, ApJ, 439, 337
Huber M. E., Everett M. E., Howell S. B., 2006, AJ, 132, 633
Johnson H. L., 1966, ARA&A, 4, 193
Lomb N. R., 1976, Ap&SS, 39, 447
Morales-Rueda L., Maxted P. F. L., Marsh T. R., North R. C., Heber U., 2003, MNRAS, 338, 752
Press W. H., Teukolsky S. A., Vetterling W. T., Flannery B. P., 1992, Numerical Recipes in C: The Art of Scientific Computing. Cambridge Univ. Press, Cambridge
Preston G. W., Shectman S. A., Beers T. C., 1991, ApJ, 375, 121
Ramsay G., Hakala P., 2005, MNRAS, 360, 314
Scargle J. D., 1982, ApJ, 263, 835
Street R. A. et al., 2005, MNRAS, 358, 795
Tyson J. A., 2002, in Tyson J. A., Wolff S., eds, Proc. SPIE Vol. 4836, Survey and Other Telescope Technologies and Discoveries. SPIE, Bellingham, p. 10

This paper has been typeset from a TEX/LATEX file prepared by the author.